Experimental Investigation of Dynamic Chip Formation in Orthogonal Cutting

Tamas G. Molnar[a,*], Szabolcs Berezvai[a], Adam K. Kiss[a], Daniel Bachrathy[a], Gabor Stepan[a]

[a]*Department of Applied Mechanics, Budapest University of Technology and Economics, H-1111 Budapest, Hungary*

Abstract

Orthogonal planing experiments are conducted with high-speed camera recordings and simultaneous cutting force measurements in order to analyze chip formation during machine tool vibrations. By means of carefully designed periodic forcing of the cutting tool, non-stationary cutting experiments are performed including wave generation, wave removal and wave-on-wave cutting, which are then compared to stationary cutting tests. The experiments are performed to address how the cutting force is affected by the chip thickness variation, the surface waviness and the fluctuation of the cutting direction. The results are used to assess some theoretical models that involve shear angle variation and chip segmentation.

Keywords: metal cutting, chip formation, chatter, cutting experiments, high-speed camera

1. Introduction

Chatter vibrations may arise in a wide range of metal cutting processes including turning [1, 2, 3], milling [4, 5, 6, 7], drilling [8], grinding [9], boring [10] and turn-milling [11]. These machine tool vibrations are known for their harmful nature that reduces the efficiency of the cutting process, the tool life and the quality of the surface finish. Although chatter has been studied for several decades, its accurate prediction based on dynamical models is still a challenge for researchers and in industry.

The difficulties in the prediction of chatter originate in the intricate nature of chip formation and the complexity of the underlying physics. A large number of factors influence the material removal process such as cutting conditions, tool and workpiece geometry and material properties. During chatter, further complications arise from the fact that chip formation is time-varying and is affected by the dynamics of the machine, which varies from one cutting setup to another.

Consequently, researchers typically simplify the analysis of chatter by introducing elementary models with few parameters that are usually identified by experiments. In order to construct these fundamental models of chip formation, stationary (chatter-free) orthogonal cutting experiments are performed. Then, time-varying chip formation is predicted (extrapolated) from the relationships obtained for stationary cutting.

The extension of stationary chip formation models to the case of dynamic (time-varying) cutting processes is not trivial. Hereinafter, the works of [12, 13, 14] are followed and simple geometric concepts are investigated to extend the stationary relationships for the study of machine tool vibrations. These geometric concepts take into account that chatter gives rise to chip thickness variation, surface waviness and cutting direction fluctuation, which affect the geometry of the chip deformation zones and hence the cutting force.

The focus of this paper is the experimental investigation of stationary and time-varying chip formation. Orthogonal planing experiments are conducted to make comparison with the chip formation theory in [12, 13, 14], and the results are interpreted from machine tool vibrations point of view. Although the planing process operates with small cutting speeds, it enables the accurate realization of various tool paths. This way, cutting force fluctuations during time-varying chip removal can be studied thoroughly.

Apart from the inspection of cutting force signals, special attention is devoted to the assessment of shear angle models and the observation of chip segmentation. These are supported by high-speed camera recordings of the chip formation process, which are rarely used by quantitative studies in the literature (for some examples, see [15, 16, 17, 18]). Although experimental results on chip formation have been published for more than half a century (see e.g. wave generation and wave cutting experiments on a lathe in [19, 20, 21, 22, 23]), today's sophisticated instruments can still provide new insights into the mechanics of metal cutting. Some recent works about high-speed camera recordings of machining processes can be found in [18, 24, 25].

The paper is organized as follows. Section 2 describes a theoretical model based on [12, 13, 14], which uses a geometrical explanation for the cutting force fluctuations. The experimental setup compiled for the planing tests is introduced in Section 3. Sections 4-6 present the results of various stationary and non-stationary cutting experiments, while conclusions are summarized in Section 7.

*Corresponding author

Email addresses: molnar@mm.bme.hu (Tamas G. Molnar), berezvai@mm.bme.hu (Szabolcs Berezvai), kiss_a@mm.bme.hu (Adam K. Kiss), bachrathy@mm.bme.hu (Daniel Bachrathy), stepan@mm.bme.hu (Gabor Stepan)

2. Basic Model of Chip Formation

In order to address the effect of machine tool vibrations on the cutting force, a basic model of dynamic (time-varying) chip formation is formulated following [12, 13, 14]. This model is used later to explain most of the experimental observations. In the model, orthogonal cutting is investigated and vibrations are considered in the feed direction only since vibrations in the nominal cutting direction are typically less significant in the models of regenerative machine tool chatter [26]. First, the tool is considered to be sharp, then remarks are given regarding the effect of the tool edge radius. The behavior of the workpiece material is approximated as elastic-perfectly plastic. Built-up edge formation is not taken into account by the model, although it may occur at small cutting speeds. Furthermore, it is assumed that there is no contact between the tool's flank face and the workpiece.

The model considers the effect of fluctuations in the cutting direction due to machine tool vibrations and the waviness of the initial surface to be cut. These have significant influence on the geometrical parameters of chip formation such as the effective cutting direction and the effective rake angle (see definitions below) and the size of deformation zones in the chip. Since these parameters strongly affect the cutting force, the term *geometrical explanation* is used when the cutting direction fluctuation and the surface waviness are taken into account to address cutting force variations. Due to its geometrical nature, this explanation could be applied to various workpiece and tool material combinations, however, the experiments of this paper are restricted to aluminum workpiece and carbide tool.

2.1. Fluctuation of the cutting direction

Let $\mathbf{v}_\mathrm{c}$ denote the *nominal* cutting velocity vector (that is parallel to the y axis in Fig. 1). When machine tool vibrations occur, it is modified by the vibration velocity $\dot{z}$, and the *effective* cutting velocity becomes $\mathbf{v}$ as indicated in Fig. 1. The direction of the effective cutting velocity, i.e., the effective cutting direction is given by the angle $\Delta\alpha$ where

$$\tan\Delta\alpha = \frac{\dot{z}}{v_\mathrm{c}}\,, \tag{1}$$

cf. Fig. 1. In what follows, the effective cutting direction is used instead of the nominal one in order to describe the dynamics of chip formation.

As a first step, the direction perpendicular to the effective cutting direction is used to determine the rake angle of the tool. Thus, the nominal rake angle α_r is modified by the effective cutting angle $\Delta\alpha$, and the effective rake angle becomes

$$\alpha = \alpha_\mathrm{r} - \Delta\alpha\,, \tag{2}$$

as shown in Fig. 1. In addition, the chip thickness should also be measured according to the effective cutting direction. Thus, the effective uncut chip thickness h_eff can be calculated as the projection of the nominal uncut chip thickness h perpendicular to the effective cutting direction:

$$h_\mathrm{eff} = h\cos\Delta\alpha\,. \tag{3}$$

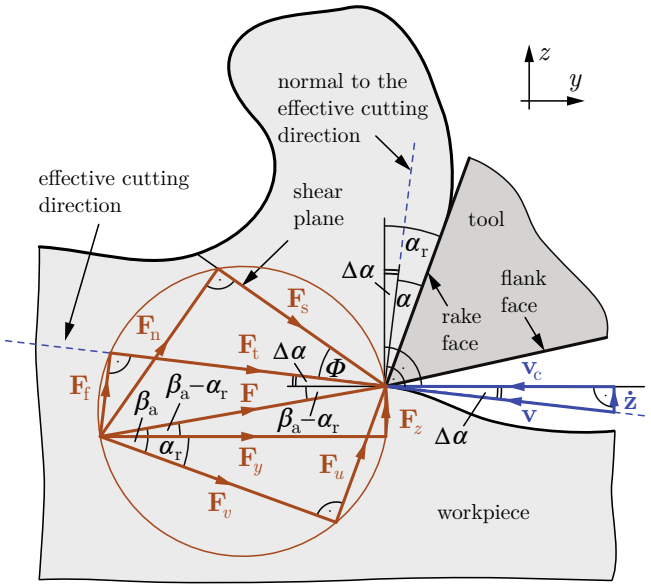

Figure 1: Illustration of the cutting velocity (blue) and the cutting force components (brown) via Merchant's circle [14]. Notice that the effective cutting velocity $\mathbf{v}$ determines the effective cutting direction (dashed line), opposed to the nominal cutting velocity $\mathbf{v}_\mathrm{c}$. The cutting force can be decomposed into four pairs of components: (i) $\mathbf{F} = \mathbf{F}_u + \mathbf{F}_v$, (ii) $\mathbf{F} = \mathbf{F}_y + \mathbf{F}_z$, (iii) $\mathbf{F} = \mathbf{F}_\mathrm{t} + \mathbf{F}_\mathrm{f}$ and (iv) $\mathbf{F} = \mathbf{F}_\mathrm{s} + \mathbf{F}_\mathrm{n}$ according to alignments to (i) the rake face, (ii) the nominal cutting direction, (iii) the effective cutting direction and (iv) the shear plane, respectively.

Note that the effective chip thickness is of less importance in this model as the shear plane length will be used instead later.

2.2. Components of the cutting force

First, the idealized case of a perfectly sharp tool with zero tool edge radius is considered. The cutting force is decomposed into various component pairs which are then used to build a cutting force model for the sharp tool. The effect of tool edge radius is addressed later in a separate subsection.

Let $\mathbf{F}$ denote the resultant cutting force acting on the tool. The direction and the components of the cutting force are illustrated in Fig. 1 via Merchant's circle [14]. On one hand, the cutting force can be decomposed into components $\mathbf{F}_u$ and $\mathbf{F}_v$ being parallel with and perpendicular to the rake face, respectively. The ratio of these components is a kind of average friction coefficient μ_a that is associated with the average friction angle β_a:

$$\mu_\mathrm{a} = \tan\beta_\mathrm{a}\,. \tag{4}$$

The direction of the cutting force is characterized by the angle β_a. This angle can be determined by measuring the y- and z-directional cutting force components F_y and F_z and by using

$$\beta_\mathrm{a} = \arctan\left(\frac{F_z}{F_y}\right) + \alpha_\mathrm{r}\,, \tag{5}$$

cf. Fig. 1.

Apart from the decompositions $\mathbf{F} = \mathbf{F}_u + \mathbf{F}_v$ and $\mathbf{F} = \mathbf{F}_y + \mathbf{F}_z$, the cutting force can be decomposed into tangential and feed components $\mathbf{F}_\mathrm{t}$ and $\mathbf{F}_\mathrm{f}$, which are aligned with and perpendicular to the effective cutting direction, respectively.

2.3. Cutting force model for sharp tools

During chip formation in orthogonal cutting, the material in front of the cutting edge is sheared over a primary shear zone [14]. This zone is approximated by the shear plane, whose length is denoted by l and whose width is the chip width w. The shear plane is located at shear angle Φ, which is measured from the effective cutting direction. Based on the shear angle Φ, the cutting force $\mathbf{F}$ can be calculated in the following manner [14].

The cutting force is decomposed into components $\mathbf{F}_\mathrm{s}$ and $\mathbf{F}_\mathrm{n}$, which are aligned with and perpendicular to the shear plane, respectively. The component $\mathbf{F}_\mathrm{s}$ is calculated from the shear stress τ_s in the shear plane. According to [20, 27, 28, 29], this shear stress is constant for a large variety of cutting conditions and is uniformly distributed over the shear plane. Thus, the shear plane-directional cutting force component becomes

$$F_\mathrm{s} = \tau_\mathrm{s} w l \,, \tag{6}$$

where wl is the shear plane area. According to Fig. 1, the magnitude of the resultant cutting force becomes

$$F = \frac{F_\mathrm{s}}{\cos(\Phi + \beta_\mathrm{a} - \alpha_\mathrm{r} + \Delta\alpha)} \,. \tag{7}$$

The y- and z-directional cutting force components that can be measured during experiments are

$$\begin{aligned} F_y &= F\cos(\beta_\mathrm{a} - \alpha_\mathrm{r}) \,, \\ F_z &= F\sin(\beta_\mathrm{a} - \alpha_\mathrm{r}) \,, \end{aligned} \tag{8}$$

while the tangential and feed components become

$$\begin{aligned} F_\mathrm{t} &= F\cos(\beta_\mathrm{a} - \alpha_\mathrm{r} + \Delta\alpha) \,, \\ F_\mathrm{f} &= F\sin(\beta_\mathrm{a} - \alpha_\mathrm{r} + \Delta\alpha) \,. \end{aligned} \tag{9}$$

2.4. Correction by considering the tool edge radius

For a real cutting tool with nonzero tool edge radius, the cutting force is the resultant of the force exerted on the tool's rake face (called *tool face force*) and the force exerted on the tool edge radius (called *ploughing force*) [30, 19, 29]. Hereinafter, the y- and z-directional components of the ploughing force are denoted by P_y and P_z, respectively. The components of the tool face force become $F_y - P_y$ and $F_z - P_z$ after subtracting the ploughing force from the total cutting force.

The cutting force model constructed above neglects the tool edge radius and the ploughing force, which makes the total cutting force equal to the tool face force. However, for nonzero tool edge radius, the total cutting force and the tool face force are different and must be distinguished. Since the model above is based on determining the force direction from the friction along the rake face, it is related rather to the tool face force than to the total cutting force. In order to obtain the total cutting force, corrections must be made to the model.

Since the average friction angle β_a is related to the direction of the tool face force, Eq. (5) must be corrected to [30]

$$\beta_\mathrm{a} = \arctan\left(\frac{F_z - P_z}{F_y - P_y}\right) + \alpha_\mathrm{r} \,. \tag{10}$$

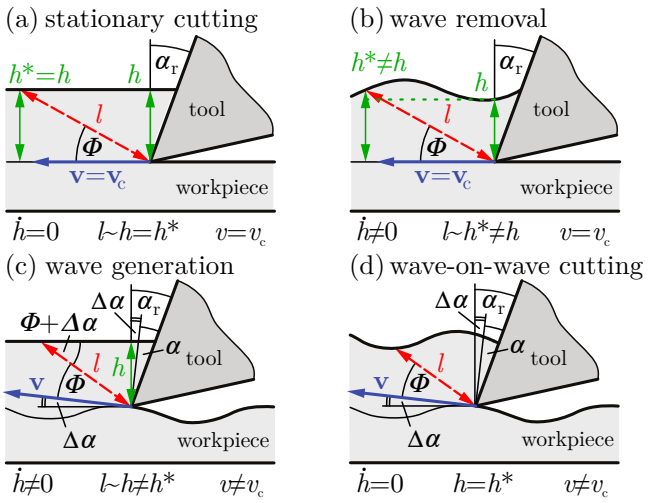

Figure 2: Illustration of (a) stationary cutting, (b) wave removal, (c) wave generation and (d) synchronous wave-on-wave cutting.

Using this angle, the formulas in Eqs. (6)-(8) can be used to obtain the tool face force (instead of the total cutting force). By adding ploughing force, the components of the total cutting force become

$$\begin{aligned} F_y &= \frac{\tau_\mathrm{s} w l}{\cos(\Phi + \beta_\mathrm{a} - \alpha_\mathrm{r} + \Delta\alpha)} \cos(\beta_\mathrm{a} - \alpha_\mathrm{r}) + P_y \,, \\ F_z &= \frac{\tau_\mathrm{s} w l}{\cos(\Phi + \beta_\mathrm{a} - \alpha_\mathrm{r} + \Delta\alpha)} \sin(\beta_\mathrm{a} - \alpha_\mathrm{r}) + P_z \,. \end{aligned} \tag{11}$$

Both for zero and nonzero tool edge radius, there are two parameters in the cutting force model, which have key importance in the subsequent analysis: the shear angle Φ and the shear plane length l, as explained in the subsequent subsection.

2.5. Shear angle models

There exist various models to characterize the shear angle Φ. The two most popular models are the maximum shear stress principle (MSSP) and the minimum energy principle (MEP) [14]. The MSSP states that the shear plane lies in the direction of maximum shear stress, which is 45° (or $\pi/4$) from the cutting force vector $\mathbf{F}$ [14]:

$$\Phi + \beta_\mathrm{a} - (\alpha_\mathrm{r} - \Delta\alpha) = \frac{\pi}{4} \,. \tag{12}$$

Meanwhile, according to the MEP, the shear angle Φ satisfies that the power $-F_\mathrm{t} v$ of the cutting force is minimal [12, 14], which leads to

$$\Phi + \frac{\beta_\mathrm{a} - (\alpha_\mathrm{r} - \Delta\alpha)}{2} = \frac{\pi}{4} \,. \tag{13}$$

Notice that for both the MSSP and the MEP, the shear angle is determined by the effective rake angle $\alpha = \alpha_\mathrm{r} - \Delta\alpha$.

In the literature, several other shear angle models can be found [31, 28, 29]. Some of them use direct empirical relationships [32], others relate the shear angle to the (empirically determined) chip compression ratio [27, 22, 32, 33], while further

models use slip-line field theory [34]. Most models claim that the shear angle fluctuates if the initial surface is wavy and/or the tool vibrates during cutting [31, 20, 13, 21, 23]. Note that the MSSP and the MEP lead to a fluctuating shear angle Φ if the cutting angle $\Delta\alpha$ fluctuates, thus the shear angle Φ depends on the vibration velocity $\dot{z}$ through Eq. (1). In this paper, we investigate whether these shear angle models – which were originally introduced for stationary cutting – give accurate cutting force predictions for non-stationary cutting. Our assumption is that the formation of the shear plane is a much faster process than the tool oscillation, thus a quasi-stationary model is adequate.

2.6. Shear plane length

The shear plane length l can be calculated from the locations of the end points of the shear plane, which are affected by machine tool vibrations. This is illustrated in Fig. 2, where four cases are considered following [12, 19, 13, 27, 21, 23, 28, 29]. Cases (a)-(b) illustrate ideal cutting without vibrations ($\mathbf{v} = \mathbf{v}_c$, $\Delta\alpha = 0$) where the tool path is a straight line and the machined surface (the lower surface of the chip) is flat without any waviness. Case (a) is called *stationary cutting* where the initial surface (the upper surface of the chip) is also flat, thus the nominal uncut chip thickness h is constant ($\dot{h} = 0$). Meanwhile, a wavy initial surface is cut in case (b) resulting in a time-varying nominal uncut chip thickness ($\dot{h} \neq 0$). This case is called *wave removal* [13, 27, 21, 23, 28, 29]. Cases (c)-(d) correspond to machine tool vibrations with wavy tool path ($\mathbf{v} \neq \mathbf{v}_c$, $\Delta\alpha \neq 0$) and wavy machined surface. Case (c), where a flat initial surface is machined and the nominal uncut chip thickness varies ($\dot{h} \neq 0$), is called *wave generation* [19, 13, 27, 21, 23, 29]. Whereas in case (d), a wavy initial surface is cut with a wavy tool path, thus this case is referred to as *wave-on-wave cutting* [19, 13]. When the waviness on the initial surface is the same as the one on the machined surface (i.e., they have the same shape, amplitude, wavelength and phase), the nominal uncut chip thickness is constant ($\dot{h} = 0$) and this case is called *synchronous* wave-on-wave cutting.

When at least one of the surfaces of the chip is flat, the shear plane length is related to the nominal uncut chip thickness at a certain position. The nominal uncut chip thickness at the tool tip is denoted by h, while the nominal uncut chip thickness at the end of the shear plane is indicated by h^*. For the stationary cutting case in Fig. 2(a), these two chip thickness values are the same ($h^* = h$), as the chip thickness is constant in time. Thus, the chip thickness is directly related to the shear plane length l:

$$l = \frac{h}{\sin\Phi} = \frac{h^*}{\sin\Phi}\,, \tag{14}$$

cf. Fig. 2(a). For the wave removal case in Fig. 2(b), the shear plane length l is related to the shifted uncut chip thickness h^* at the end of the shear plane (and *not* to the nominal uncut chip thickness h at the tool tip):

$$l = \frac{h^*}{\sin\Phi}\,, \tag{15}$$

cf. Fig 2(b). For the wave generation case in Fig. 2(c), the cutting velocity $\mathbf{v}$ fluctuates as it is tangent to the wavy tool path.

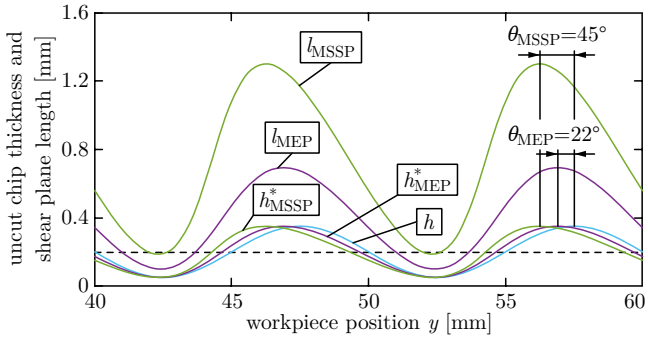

Figure 3: (a) Illustration of the nominal uncut chip thickness h at the tool tip, the shifted uncut chip thickness h^* at the end of the shear plane and the shear plane length l assuming the MSSP and the MEP shear angle models for the case of wave removal (see Fig. 2(b)). The figure corresponds to an orthogonal planing experiment (see details in Sec. 5) where wave removal took place with rake angle $\alpha_r = 2.5°$, cutting speed $v_c = 5$ m/min, mean chip thickness $h_{\mathrm{mean}} = 200\ \mu$m, chip thickness amplitude $h_{\mathrm{amp}} = 150\ \mu$m and wavelength $\lambda = 10$ mm. Notice the phase shift θ between h and h^*, h and l.

The cutting angle $\Delta\alpha$ should be taken into account when calculating the shear plane length, which is related to the nominal uncut chip thickness h at the tool tip:

$$l = \frac{h}{\sin(\Phi + \Delta\alpha)}\,. \tag{16}$$

For the wave-on-wave cutting case in Fig. 2(d), there is no direct relationship between the shear plane length l and the chip thicknesses h or h^*. The length of the shear plane can be calculated numerically from the coordinates of its end points.

2.7. Phase shift between cutting force and chip thickness

According to theoretical models [19, 13, 28, 29, 33] and experiments [35, 19, 27, 21] (see later also in Sec. 5), there is a noticeable phase shift between the cutting force and the nominal uncut chip thickness if the latter is time-varying. Typically, a geometrical explanation is given to address this phase shift, although some papers indicate that geometric relations alone are insufficient to describe dynamic cutting due to the complicated underlying physics [34].

For wave generation, the geometrical explanation [12, 13, 14] is based on the fact that the cutting direction fluctuates (see Eq. (1)). This causes fluctuations in the effective rake angle, the effective chip thickness, the shear angle and the shear plane length [27] as taken into account by Eqs. (2)-(3), (12)-(13) and (16). Fluctuations may also occur in the effective clearance angle, in the cutting speed [27, 21, 23] and even in the shear stress in the shear plane [33], which are neglected here. In the end, the cutting force depends on the vibration velocity $\dot{z}(t)$ through Eq. (11). Since for a harmonic tool position $z(t)$, the velocity $\dot{z}(t)$ is in 90° phase shift with respect to the position, the velocity dependency causes a phase shift between the cutting force and the chip thickness variation, where the force leads the chip thickness. In [13], a formula can also be found for the phase shift. Note that the velocity dependency drops when considering the MSSP shear angle expression, since the

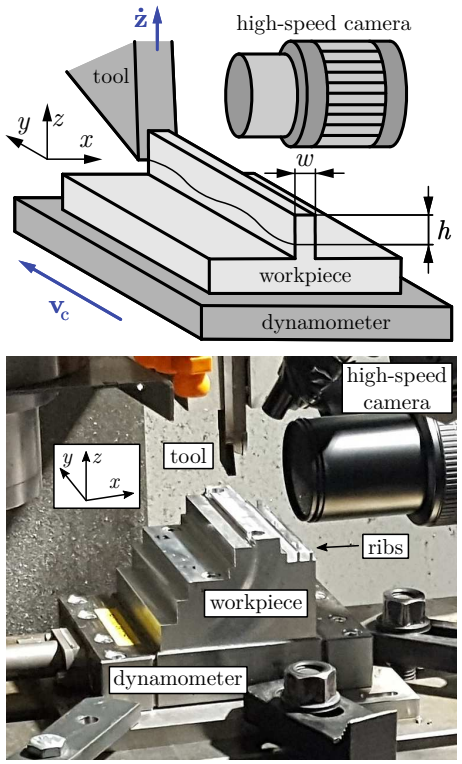

Figure 4: Schematic representation and photo of the experimental setup for orthogonal planing tests.

angle $\Phi + \Delta\alpha$ is constant (velocity-independent) according to Eq. (12). Thus, in this approach, the MSSP is not able to explain the phase shift between the cutting force and the chip thickness in wave generation, while the MEP has no such deficiency.

As for wave removal, the geometric explanation for the phase shift is different [35, 13]. In this case, the cutting direction is *not* fluctuating ($\Delta\alpha = 0$), the effective chip thickness is the same as the nominal one ($h_{\text{eff}} = h$), there are no velocity-dependent fluctuations in the rake angle ($\alpha = \alpha_{\text{r}}$) or in the shear angle (Φ is constant according to Eqs. (12)-(13)). However, the shear plane length is now given by Eq. (15) and it is related to the shifted uncut chip thickness h^* (see Fig. 2(b)). Since the shifted uncut chip thickness h^* is ahead of the nominal one h with respect to the tool's motion, h^* has a phase lead compared to h (see the corresponding formula given in [13]). This is illustrated in Fig. 3, where the uncut chip thickness values of an actual cutting test are depicted (details of the experiment are given in Sec. 5). Here, the shifted uncut chip thicknesses h^*_{MSSP} and h^*_{MEP} were calculated numerically from the prescribed tool path using the shear angle from the MSSP and MEP models, respectively. Figure 3 shows the corresponding shear plane lengths l_{MSSP} and l_{MEP} as well. The shear plane lengths – and the cutting forces related to them – also exhibit a phase shift with respect to the nominal uncut chip thickness h and the relationship of l and h is nonlinear. As shown later amongst the experimental results, the MSSP typically predicts a larger shear plane length and a larger phase shift than the MEP does in wave removal.

The phase shift between cutting force and chip thickness is typically larger for wave removal than for wave generation, and typically increases for increasing chip thickness variation and decreasing rake angle. The observation of this phase shift will play an important role in the experiments described in Sec. 5.

3. Experimental Setup

In the rest of the paper, the cutting force is investigated experimentally for dynamic (time-varying) chip formation. Cases (a)-(d) of Fig. 2 are studied systematically in order to investigate the effects of chip thickness variation (occurring in cases (b) and (c)), surface waviness (cases (b) and (d)) and fluctuation of the cutting direction (cases (c) and (d)) on the cutting force. Note that all of these effects occur simultaneously in actual machining processes in the presence of chatter. Here, the early work of Albrecht [12] is followed, where the theoretical analysis of cases (a)-(d) was discussed similarly to Sec. 2. The present work contributes to the literature, on the one hand, by the direct analysis of cutting force signals with special attention to the chip segmentation phenomenon and to the analysis and explanation of the cutting force characteristics during dynamic cutting. On the other hand, emphasis is put on the assessment of shear angle models and the results are also supplemented by high-speed camera recordings of the cutting process.

In order to investigate chip formation, dry orthogonal planing tests were performed. The experimental setup is shown in Fig. 4. Ribs were prepared on an aluminum (A2024-T351) workpiece and were machined using carbide cutting tools. Tool coating and lubricant were not used in these experiments. The length of the ribs was 100 mm, the width of the ribs (i.e., the chip width) was $w = 2$ mm, while the width of the cutting tool was 5 mm. Four tools with rake angle $\alpha_{\text{r}} = 2.5°,\ 5°,\ 10°$ and $15°$ were used, while the flank angle was $10°$ for each tool. The tool edge radius was measured by microscope and was found to be 13, 15, 26 and 34 μm, respectively.

Note that the initial fast wearing of the tools had already taken place before measuring the tool edge radius and starting the experiments of this work. The presented set of experiments involves about 100 cutting tests for each tool. Since in the planing process the total length of the workpiece material cut by a single tool is small (for example, much smaller compared to turning experiments), we did not experience any noticeable tool wear during the experiments. Accumulated built-up edge formation was also avoided by cleaning the tool and removing the remains of the chip from the tool after each cut. If there was built-up edge formation during a single cut, it could be observed by high-speed camera or by significant changes in the cutting force signal. Biased experimental results affected by significant built-up edge formation were disregarded.

For the cutting tests, the workpiece was mounted on the table of an NCT EmR-610Ms CNC milling machine as shown in Fig. 4. The nominal cutting speed was provided by the feed motion of the machine via moving the workpiece in the y direction. The nominal cutting speed was set to $v_{\text{c}} = 5,\ 10$ and 30 m/min. These low cutting speed values were chosen due to the speed constraints of the machine and in order to investigate the chip segmentation phenomenon discussed later. Before

each cutting test, 120 mm space was provided for accelerating the workpiece, while 60 mm space was used for deceleration. The tool was mounted on (and moving together with) the house of the main spindle of the CNC milling machine. Vibrations during cutting were imitated by moving the tool in the z direction, which enabled the generation of various tool paths (with a command rate of 500 Hz). Sinusoidal tool paths were used to generate fluctuating cutting force in cases (b)-(d) of Fig. 2.

In order to verify the accurate realization of the prescribed tool motion, the tool position was queried from the CNC milling machine with a sampling frequency of 1000 Hz. The cutting force components were measured in the (x, y, z) coordinate system (see Fig. 4) by mounting the workpiece on a Kistler 9129AA multicomponent dynamometer, and the data were acquired using a 5080A charge amplifier and four NI-9234 Input Modules in a NI cDAQ-9178 Chassis at 51200 Hz sampling frequency. The chip formation process was recorded by a Photron FASTCAM SA5 High-Speed Camera System with 7000 frames per second and resolution of 1024×1024 pixels. Canon MP-E 65 mm macro lens with 5:1 magnification were used to magnify the observed area during recording. In order to meet the strict lighting requirements of the high-speed camera, two Vision Device VD7000 LED lamps and an endoscope-like Hayashi HDF7010 Fiber Optic LED system were applied. For more details on the high-speed camera measurement setup, the reader is referred to [18, 36, 37]. A video about the high-speed camera recordings can be found under http://siren.mm.bme.hu/Videoblog.html.

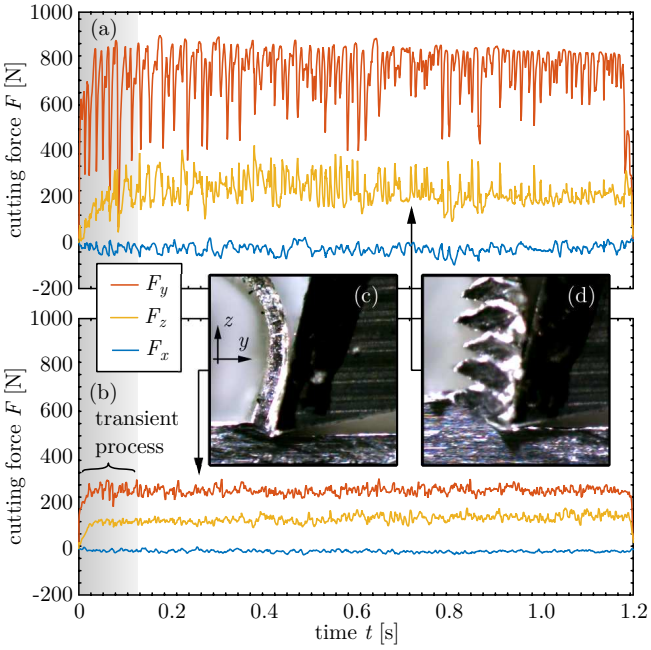

Figure 5: Cutting force signals for stationary planing processes (case (a) of Fig. 2). The rake angle was $\alpha_r = 10°$, the nominal cutting speed was $v_c = 5$ m/min and the nominal uncut chip thickness was (a) $h = 400\ \mu$m, (b) $h = 100\ \mu$m. The light gray shaded region indicates the transient process before reaching the steady state cutting process. The typical shapes of a continuous and a segmented chip are shown in panels (c) and (d), respectively.

4. Experimental Results for Stationary Cutting

First, stationary cutting (case (a) of Fig. 2) was considered, where the initial surface is flat and only the workpiece is moving along the y direction, which generates a straight line tool path and a constant nominal uncut chip thickness. In this case, certain cutting force components coincide: the y-directional $\mathbf{F}_y$ and the tangential $\mathbf{F}_t$, as well as the z-directional $\mathbf{F}_z$ and the feed directional $\mathbf{F}_f$. A sequence of experiments were performed for rake angles $\alpha_r = 2.5°,\ 5°,\ 10°$ and $15°$, nominal cutting speeds $v_c = 5,\ 10$ and 30 m/min, and 22 different nominal uncut chip thickness values ranging from 10 μm to 500 μm.

Figure 5(a-b) show an example for the measured cutting force signals that act on the tool as a function of time for a large ($h = 400\ \mu$m) and a small ($h = 100\ \mu$m) nominal uncut chip thickness value (with $\alpha_r = 10°$ and $v_c = 5$ m/min). In both cases, the cutting force components undergo a short transition (see shaded region) until reaching their steady state, which may be caused by thermal processes or by the flexibility (slight deformation) of the tool holder structure.

According to the experiments, the phenomenon of chip segmentation occurs for large chip thickness values: the chip thickness fluctuates although its nominal value is constant. The typical shapes of a continuous and a segmented chip are shown in the high-speed camera pictures of Fig. 5(c-d). The segmentation phenomenon is also clearly indicated by the sharp peaks of the cutting force signal in Fig. 5(a). Namely, there is a repeated abrupt decrease in the y-directional (tangential) cutting force component and a repeated abrupt increase in z-directional (feed) component during segmentation. That is, the frequent peaks in the cutting force signal do not indicate the noise of the measurement, but are related to the physics of chip formation. Note that the dynamics of the dynamometer also causes high frequency components in the force signal, but these were removed using the method introduced in [38].

The segmentation-induced cutting force fluctuation is negligible for the small chip thickness value in Fig. 5(b). The explanation of chip segmentation is out of scope of this paper, although there exist several physical models in the literature [39, 40, 41, 42, 43]. Here, the occurrence of segmentation is investigated based on the inspection of the cutting force signal and the high-speed camera recordings only. According to the sequence of cutting tests, segmentation is more likely to occur (and has larger effect on the cutting force) when the nominal uncut chip thickness is large. *Slight segmentation* takes place for uncut chip thickness values $h \gtrsim 150\ \mu$m. This is associated with small variations in the deformed chip thickness and small, less abrupt fluctuations in the cutting force. For larger chip thickness values, $h \gtrsim 300\ \mu$m, *strong segmentation* evolves, which is accompanied by peculiar sharp peaks in the cutting force signal. The tangential cutting force and the deformed chip thickness repeatedly drops in this case, sometimes even nearly to zero. The chip thickness associated with the onset of segmentation typically increases with increasing cutting speed and rake angle for the cutting parameter ranges considered in the experiments. Furthermore, it was also observed that

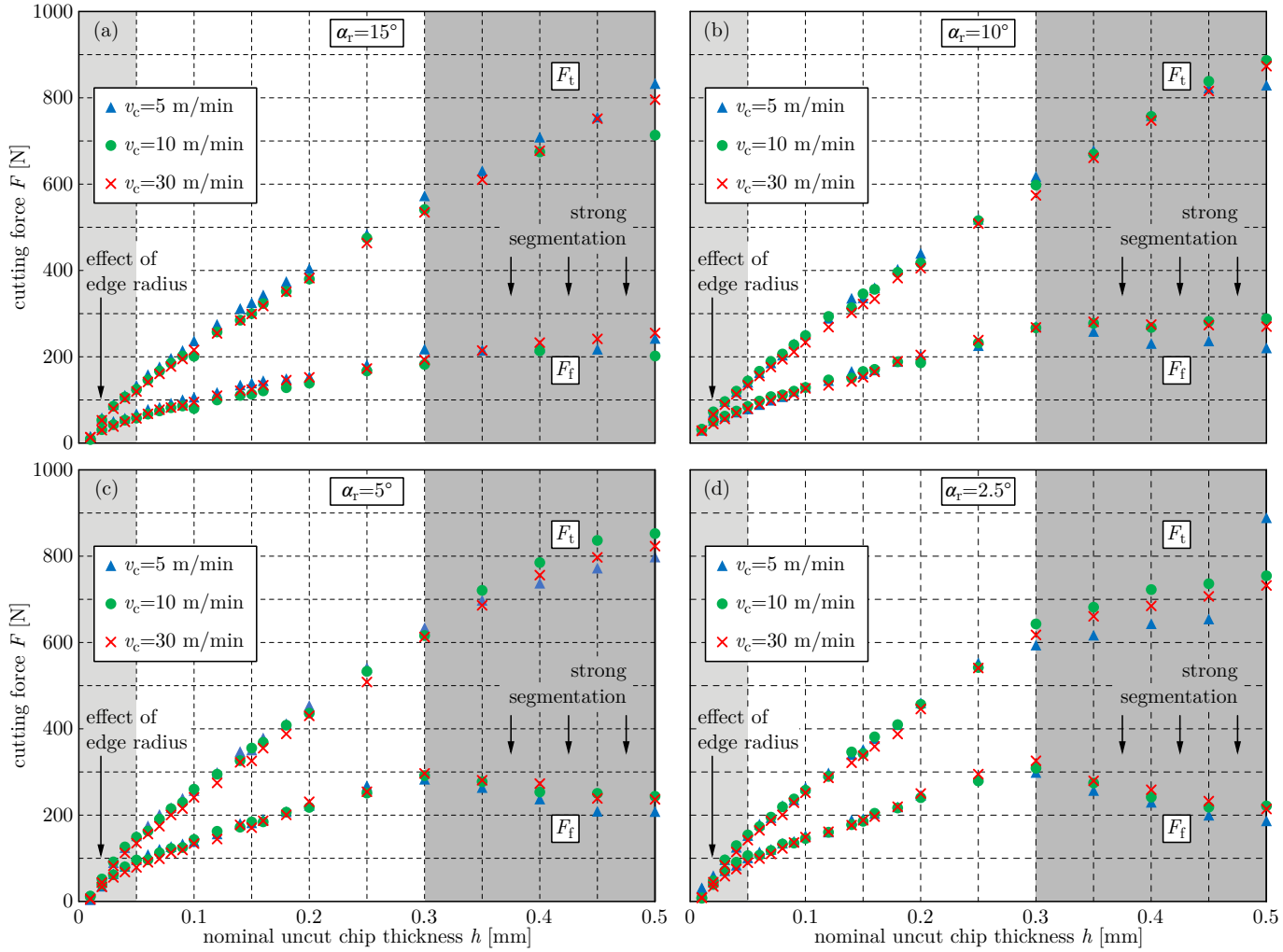

Figure 6: Average tangential and feed cutting force components as a function of the nominal uncut chip thickness for nominal cutting speeds v_c = 5, 10 and 30 m/min and for rake angle (a) α_r = 15°, (b) α_r = 10°, (c) α_r = 5° and (d) α_r = 2.5°. Gray shading indicates the regions where the cutting force characteristics qualitatively change and deviate from linear due to the effect of the tool edge radius (light gray) or due to strong chip segmentation (dark gray).

the higher the cutting speed is, the higher the frequency of segmentation is: the corresponding wavelength is roughly the same but the cutting takes less time for higher cutting speeds.

For each stationary cutting test, the middle third of the force signals was averaged. The characteristics of the average cutting force components as a function of the nominal uncut chip thickness are shown in Fig. 6(a-d) for α_r = 15°, 10°, 5° and 2.5°, respectively. The tangential and feed force characteristics can be approximated by a (shifted) linear function in a wide range of chip thicknesses (50 μm < h < 300 μm). This linear tendency is assumed in most cutting force models [20, 14] and it is also captured by the model of Sec. 2. Namely, the cutting force components F_y and F_z given by Eqs. (11) and (14) consist of a term proportional to the nominal uncut chip thickness h (which is the tool face force) and a constant term (the ploughigh force). This allows one to determine the values of the ploughing force components P_y and P_z by fitting straight lines to the linear range (50 μm < h < 300 μm) of the cutting force characteristics and finding their intersection with the vertical axis. The ploughing force components were determined by this method for each of the cutting force characteristics in Fig. 6 separately. The particular ploughing force values were the following:

P_y = 61, 49, 44 N and P_z = 51, 39, 38 N for α_r = 15°,
P_y = 58, 65, 47 N and P_z = 53, 59, 43 N for α_r = 10°,
P_y = 65, 60, 49 N and P_z = 60, 58, 40 N for α_r = 5°,
P_y = 61, 61, 49 N and P_z = 58, 55, 41 N for α_r = 2.5°

for cutting speeds v_c = 5, 10, 30 m/min, respectively. Note that the ploughing force strongly depends on the tool edge radius and the choice of the tool. The ploughing force values were used later to apply the model of Sec. 2 to the case of time-varying cutting. It is important that the cutting force predictions of this model are accurate in the range of medium uncut chip thickness (50 μm < h < 300 μm) only, where the cutting force versus chip thickness relationship is linear.

In other ranges of the nominal uncut chip thickness h, the cutting force characteristics are nonlinear. For small chip thickness values ($h \leq 50$ μm), the characteristics decrease in an exponential fashion [44] due to the effect of the tool edge radius (see

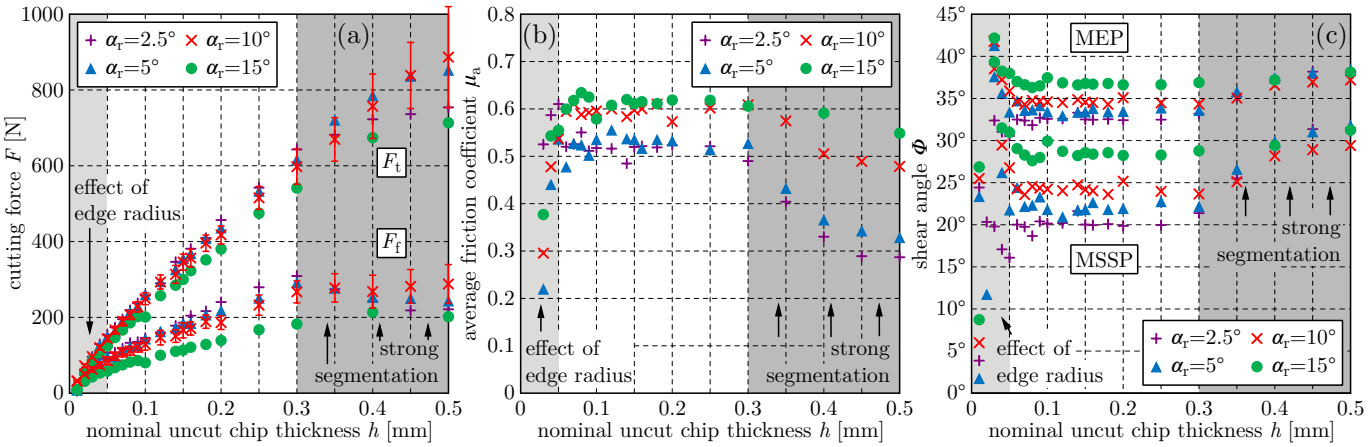

Figure 7: Characteristics of (a) the cutting force, (b) the friction coefficient and (c) the shear angle as a function of the nominal uncut chip thickness for nominal cutting speed v_c = 10 m/min and for rake angles α_r = 2.5°, 5°, 10° and 15°. The regions affected by the tool edge radius and strong chip segmentation are indicated by light and dark gray shadings, respectively.

the light gray shaded region). The cutting force drops to zero for zero chip thickness, since the tool is no longer in contact with the workpiece. It is important to note that in this region the ploughing force strongly depends on the value of the chip thickness, therefore the theoretical model of Sec. 2 (which assumes a constant ploughing force) is not applicable. Modeling cutting forces for chip thicknesses in the range of the tool edge radius is out of scope of this paper.

For large chip thicknesses ($h \geq 300\ \mu$m), a slight degressive tendency can be observed on the characteristics of the tangential force, while the feed force characteristics may break down and decrease (see the dark gray shaded region). This break down (around $h = 300\ \mu$m) can be predicted and explained by theoretical shear zone models [39, 40, 41, 42, 43], and a similar break down was observed directly in [43]. The break down is more pronounced for small cutting speeds and small rake angles, since it is associated with chip segmentation, which becomes noticeably more significant at these large chip thickness values. Note that the characteristics of the tangential and the feed forces are qualitatively different [45], which is often neglected in cutting force models used for analyzing machine tool chatter [14].

Analyzing experimental results from point of view of explaining the physics of chip segmentation is out scope of this paper. Still, for the sake of completeness, some experimental results are presented for large uncut chip thickness values subject to segmentation ($h \geq 300\ \mu$m, see the dark gray shaded region in Fig. 6). These experiments show the domain of applicability of the theoretical model of Sec. 2, which is restricted to medium chip thickness values ($50\ \mu\text{m} < h < 300\ \mu$m, see the white region in Fig. 6).

According to Fig. 6, the cutting speed has moderate effect on the cutting force magnitude (at least in the investigated range of parameters), while the effects of the rake angle and the chip thickness are more pronounced [23]. Thus, the cutting speed $v_c = 10$ m/min is selected for further analysis. For this cutting speed, the cutting force characteristics are summarized in Fig. 7(a). Note that the cutting force components typically decrease with increasing rake angle. Figure 7(a) also shows the standard deviation of the cutting force components during each cutting test with $\alpha_r = 10°$ (see the error bars). The increase of the standard deviation at large uncut chip thickness values ($h \geq 300\ \mu$m) clearly reflects the occurrence of strong chip segmentation.

Meanwhile, the average friction coefficient was also calculated from the average of the measured cutting force components using Eqs. (4) and (10). According to Fig. 7(b), the friction coefficient is approximately constant in the medium range of uncut chip thicknesses ($50\ \mu\text{m} < h < 300\ \mu$m) and its value is around $0.5 \leq \mu_a \leq 0.6$. Similar results were reported in [30]. This justifies that using a constant friction coefficient is a good approximation in this range of parameters. Note, however, that the friction coefficient is in fact varying along the tool-chip interface [46]. For large chip thickness values ($h \geq 300\ \mu$m), the friction coefficient decreases with increasing chip thickness. For small chip thickness values in the range of the tool edge radius ($h \leq 50\ \mu$m), the calculated friction coefficient is not meaningful, since Eq. (10) describes the case where the tool face force is present. Also note that the friction coefficient increases with the rake angle. Further friction properties and empirical formulas for the friction coefficient can be found in [30, 31, 32, 28, 29, 46]. In what follows, the oscillations of the friction coefficient [20] are neglected and the mean friction angle β_a is used even in non-stationary cutting.

Furthermore, the average shear angle Φ was calculated from the average friction angle β_a using the MSSP model (12) and the MEP model (13) as depicted in Fig. 7(c). Again, these results are meaningful outside the range of the tool edge radius only. The average shear angle is approximately a constant function of the uncut chip thickness in the range $50\ \mu\text{m} < h < 300\ \mu$m. The shear angle increases with the rake angle, and the MEP predicts larger shear angle than the MSSP does. Meanwhile in the range $h \geq 300\ \mu$m, the average shear angle increases with the chip thickness and there are large shear angle fluctuations around the

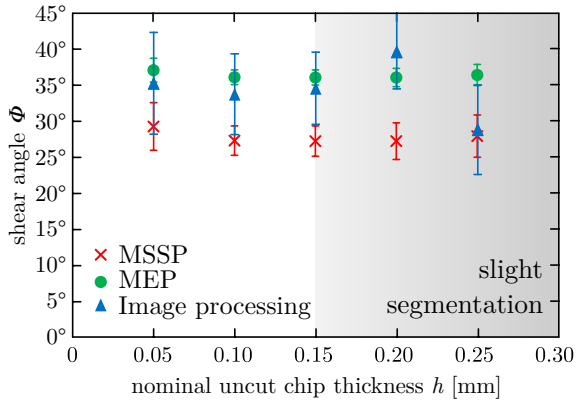

Figure 8: Comparison of the shear angle detected from high-speed camera measurements via image processing techniques and the shear angle calculated from the cutting force signals via the MSSP and the MEP shear angle models [18, 36]. The cutting conditions are $\alpha_r = 15°$ and $v_c = 10$ m/min.

average due to strong chip segmentation. Note that the shear angle predictions based on the MSSP and the MEP gradually lose validity as segmentation becomes more intensive.

In order to test the applicability of the MSSP and the MEP, the shear angle was determined also from high-speed camera recordings via image processing techniques. Planing experiments with $\alpha_r = 15°$, $v_c = 10$ m/min and $h = 50,\ 100,\ 150,\ 200,\ 250\ \mu$m were recorded. The shear angle was determined by calculating the displacement field of the chip's motion from two subsequent frames and applying Wiener-filtering. The details and results of this analysis are published in [18, 36]. The mean value and the standard deviation of the shear angle during the particular cutting tests are depicted in Fig. 8. For comparison, the shear angle values calculated from the cutting force signals via the MSSP and the MEP are also shown. The results of the MEP and the image processing are in excellent agreement for small uncut chip thickness values. For larger chip thicknesses, the accuracy of the MEP decreases due to the gradual onset of slight chip segmentation. In contrast, the MSSP underestimates the shear angle for the whole range of chip thicknesses. Note that the chip segmentation phenomenon is well-observable in high-speed camera recordings, see Fig. 5(c,d).

Finally, the shear stress τ_s in the shear plane can also be obtained from Eq. (11) using the MSSP or the MEP. The distribution of the shear stress over the different measurements is shown in the histogram of Fig. 9 for $\alpha_r = 2.5°$, $v_c = 5$ m/min. In Fig. 9(a), results are indicated for the whole set of experiments ($10\ \mu\text{m} \le h \le 500\ \mu$m, 22 measurements), while in Fig. 9(b), experiments are considered in the medium chip thickness range only without including the effect of tool edge radius and strong chip segmentation ($50\ \mu\text{m} < h < 300\ \mu$m, 12 measurements). According to Fig. 9, the assumption that the shear stress is constant regardless the cutting conditions yields a good approximation, since the distribution of the shear stress is narrow with a well-defined mean value. Based on the comparison of the two panels, deviations in the calculated shear stress can

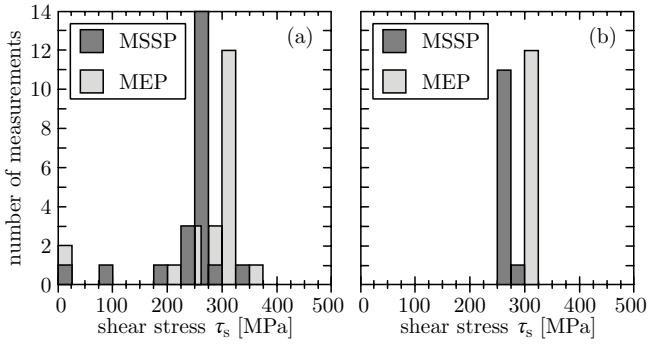

Figure 9: Distribution of the shear stress over the set of experiments with $\alpha_r = 2.5°$, $v_c = 5$ m/min and (a) $10\ \mu\text{m} \le h \le 500\ \mu$m (22 measurements), (b) $50\ \mu\text{m} < h < 300\ \mu$m (12 measurements).

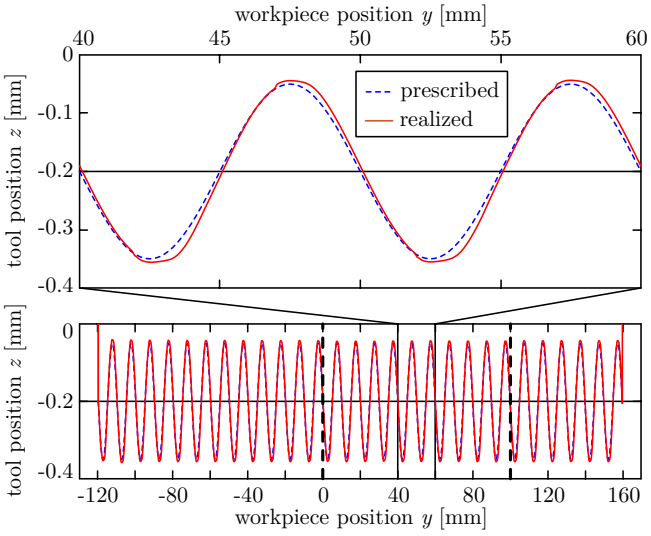

Figure 10: Prescribed and realized tool paths in wave generation for $\alpha_r = 2.5°$, $v_c = 5$ m/min, $h_{mean} = 200\ \mu$m, $h_{amp} = 150\ \mu$m, $\lambda = 10$ mm.

be attributed to the effects of tool edge radius and strong chip segmentation by which the model of Sec. 2 loses validity. Besides, the MSSP gives a smaller mean shear stress value than the MEP does.

5. Experimental Results for Sinusoidal Tool Path

After the stationary cutting tests, cases (b)-(c) of Fig. 2 were considered by performing wave generation and wave removal pairs of planing experiments. During wave generation, the initial surface was flat, the workpiece was moving in the y direction with constant speed, while the tool was moving up and down sinusoidally in the z direction (see Fig. 2(c)). This generated sinusoidal tool path and sinusoidal nominal uncut chip thickness. During wave removal, the sinusoidal wavy surface was cut by generating a straight line tool path with workpiece motion only (see Fig. 2(b)). The nominal uncut chip thickness was again sinusoidal but the tool was not moving in this case.

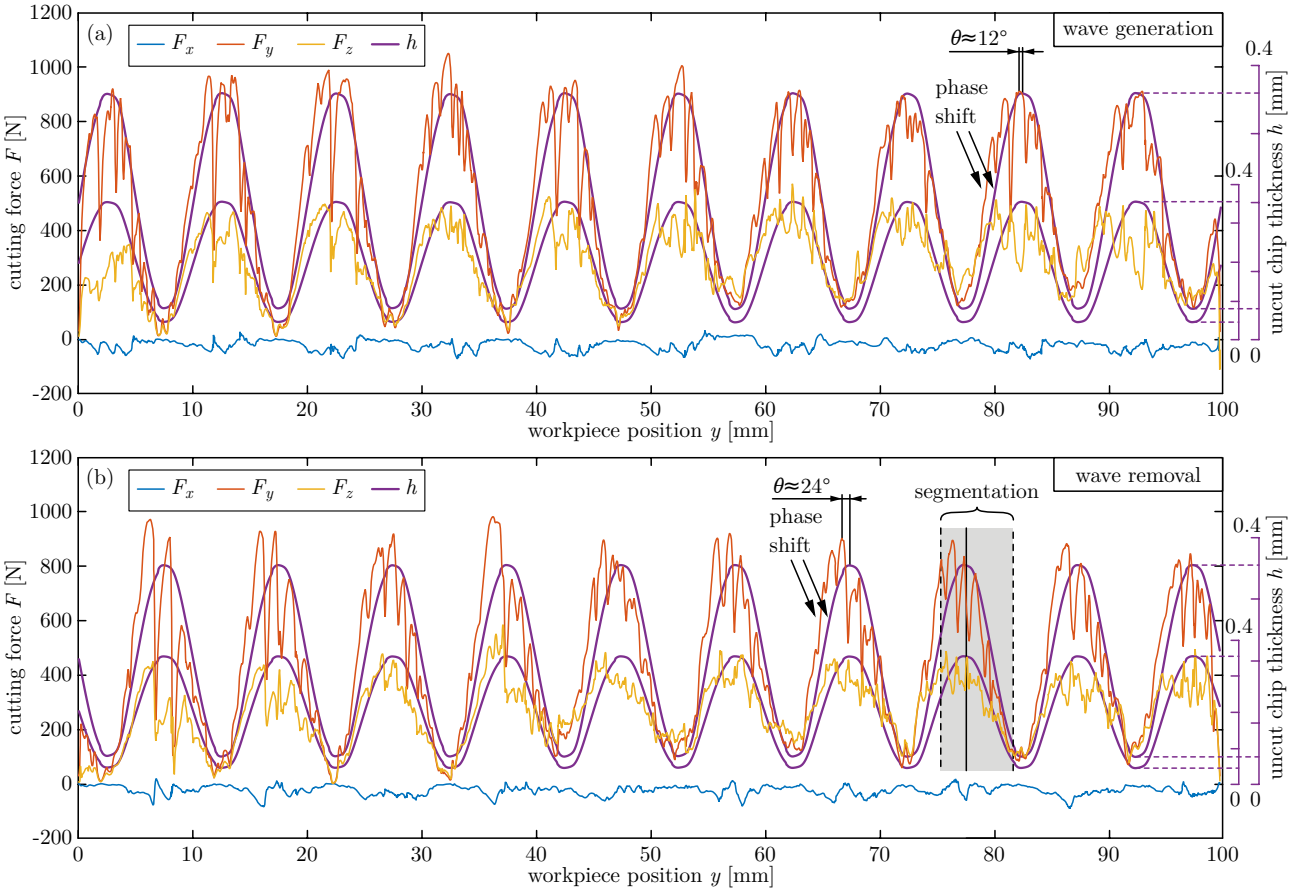

Figure 11: Cutting force signals for sinusoidal chip thickness variation (a) for wave generation (see Fig. 2(c)), (b) for wave removal (see Fig. 2(b)). The realized uncut chip thickness h is also shown by purple lines on two different scales for comparison with the cutting force components F_y and F_z. The corresponding cutting conditions are $\alpha_r = 2.5°$, $v_c = 5$ m/min, $h_{mean} = 200\,\mu$m, $h_{amp} = 150\,\mu$m, $\lambda = 10$ mm.

Results are presented for sinusoidal chip thickness variations of wavelength $\lambda = 10$ mm. Several combinations of mean values $h_{mean} = 100,\ 150,\ 200,\ 250\,\mu$m and amplitudes $h_{amp} = 50,\ 100,\ 150,\ 200\,\mu$m were considered for the nominal uncut chip thickness. In wave generation, these amplitudes correspond to $\pm\Delta\alpha_{amp}$ fluctuation of the cutting direction, where $\Delta\alpha_{amp} \approx \tan\Delta\alpha_{amp} = h_{amp}2\pi/\lambda = 1.8°,\ 3.6°,\ 5.4°,\ 7.2°$. Since the flank angle was 10°, this fluctuation did not cause any additional contact between the machined surface and the flank face of the tool, which would have strongly affected the cutting force. Note that the flank contact is related to the so-called process damping effect, which has an extensive literature [35, 47, 48, 49, 14, 50, 51, 52, 53].

The cutting speed was kept at $v_c = 5$ m/min to ensure the accurate realization of the desired (prescribed) tool path when the tool was moving. The desired sinusoidal tool path and the one generated by (and queried by) the machine are shown in Fig. 10 for $h_{mean} = 200\,\mu$m, $h_{amp} = 150\,\mu$m. The start and end of cut were at $y = 0$ and $y = 100$ mm as indicated by the thick dashed lines. It can be seen that there was a slight discrepancy between the desired and realized tool paths due to friction when the tool's motion changed direction. Therefore, the actual non-sinusoidal uncut chip thickness (calculated from the measured tool position) was used for further analysis instead of the desired sinusoidal one. However, the effective cutting direction was still approximated by the tangent of the prescribed sinusoidal tool path instead of the measured non-sinusoidal one in order to avoid the noise arising from the numerical differentiation of measured data.

Examples for the measured cutting force signal are shown in Fig. 11. Panel (a) shows a wave generation test (associated with Fig. 2(c)), while panel (b) shows wave removal (corresponding to Fig. 2(b)). For both measurements, the rake angle was $\alpha_r = 2.5°$, the nominal cutting speed was $v_c = 5$ m/min and the chip thickness was varying sinusoidally around $h_{mean} = 200\,\mu$m with amplitude $h_{amp} = 150\,\mu$m and wavelength $\lambda = 10$ mm. Scaled values of the uncut chip thickness h calculated from the tool's position are also shown by purple lines in the figure. This enables the comparison of cutting force and chip thickness signals and the observation of their phase shift.

Based on the inspection of force signals (such as the one in Fig. 11) for the series of cutting tests, the following conclusions could be drawn. The measured cutting force signals (especially F_z) become distorted and non-sinusoidal for large mean uncut chip thicknesses. Besides, chip segmentation may occur (see the peaks of the force), which is more likely for large chip

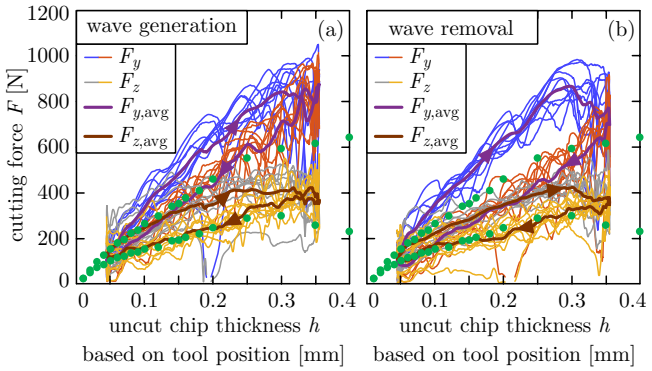

Figure 12: Characteristics of the cutting force as a function of the time-varying uncut chip thickness (a) for wave generation (b) for wave removal. For reference, dots indicate the results of the corresponding stationary cutting experiments. The cutting conditions are the same as in Fig. 11.

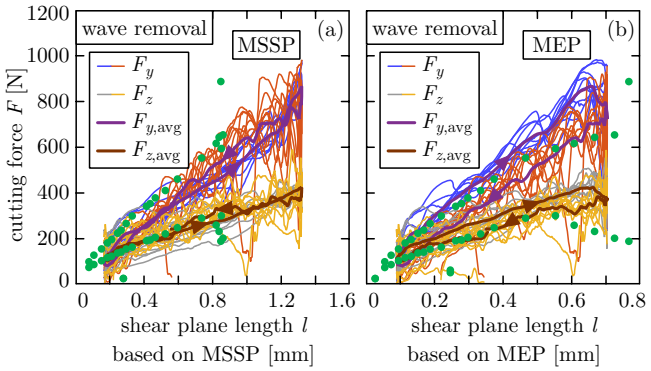

Figure 13: Characteristics of the cutting force as a function of the shear plane length calculated from (a) the MSSP (b) the MEP shear angle model for wave removal. For reference, dots indicate the results of the corresponding stationary cutting experiments. The cutting conditions are the same as in Fig. 11. Note the different scales of the horizontal axes in the two panels.

thicknesses and small rake angles, similarly to stationary cutting. In non-stationary cutting, the occurrence of chip segmentation typically exhibits hysteresis with respect to the variation of the uncut chip thickness. Namely, when the uncut chip thickness increases, segmentation begins at larger chip thickness values, and when the uncut chip thickness decreases, segmentation persists for smaller chip thickness values. This hysteresis can clearly be observed in the shaded region of Fig. 11(b). Usually segmentation and its hysteresis are more pronounced for wave removal than for wave generation, and the hysteresis is better visible for large chip thickness amplitudes.

The hysteresis of chip segmentation can be predicted by the bifurcation analysis of nonlinear shear zone models [40, 41, 42]. That is, the hysteresis may indicate the presence of nonlinearities in the process. In this sense, the hysteresis of chip segmentation is analogous to the hysteresis in the occurrence of machine tool chatter, which is caused by the (nonlinear and nonsmooth) flyover effect [54]. In both cases, process nonlinearities lead to a bistable behavior: switching occurs between two stable states (continuous chip formation and chip segmentation or chatter-free behavior and machine tool chatter), which takes place with hysteresis.

In addition, a slight phase shift can be observed in Fig. 11: the uncut chip thickness is delayed with respect to the cutting force signal. For wave removal (Fig. 11(b)), the phase shift is typically more significant. This phase shift is also shown in Fig. 12(a,b), where the cutting force components are plotted against the uncut chip thickness for wave generation and wave removal, respectively. Different colors distinguish cutting force components corresponding to increasing and decreasing uncut chip thickness. As the chip thickness varies periodically, the force signals sweep across the cutting force characteristics multiple times. In this case, the nominal uncut chip thickness consists of 10 periods, thus force signals can be separated into 10 corresponding segments. The average of the 10 segments gives an average cutting force characteristics, which are indicated by thick lines in Fig. 12 and are denoted by $F_{y,\mathrm{avg}}$ and $F_{z,\mathrm{avg}}$ for the y- and z-directional components, respectively. These thick lines show that closed curves appear in the cutting force characteristics instead of single-valued functions, which clearly indicates the presence of a phase shift between cutting force and uncut chip thickness. Since the measured force signals circle around the closed curves in the clockwise direction (see the arrows), the cutting force leads the uncut chip thickness. The closed curves typically enclose larger area in case of wave removal and large chip thickness amplitudes.

Similar closed curves in the cutting force characteristics were reported in [12, 55]. Such closed curves may indicate the dependence of the cutting force on the time-derivative $\dot{h}$ of the uncut chip thickness, which is associated with the velocity of the tool. Velocity dependency has great significance in the dynamical models of machine tool chatter. Linearization of a velocity-dependent cutting force expressions leads to an additional damping force, which affects the stability of machining and the onset of chatter. In many theoretical models, the additional damping is considered to be inversely proportional to the nominal cutting speed and is called process damping [47, 56, 48, 49, 50, 51, 52, 53]. Process damping strongly affects the occurrence of chatter at low cutting speeds: it makes the maximum stable (chatter-free) depth of cut larger as the spindle speed is decreased, which was also observed in several experiments in the literature [47, 56, 49, 57, 50, 53]. This low speed stability improvement phenomenon can also be captured by considering the distribution of the cutting force along the rake face of the tool [58, 59, 55]. Distributed cutting force models also show phase shift between the cutting force and the nominal uncut chip thickness. Therefore, understanding the origin of the phase shift is crucial in terms of relating cutting force expressions to process damping models and distributed cutting force models.

As discussed in Sec. 2, there exist a geometrical explanation for this phase shift. Recall that for wave generation, the geometrical explanation of the phase shift was based on the dependency of the cutting force on the vibration velocity due to the fluctuation of the cutting direction. While this explanation works properly with the MEP shear angle model, the MSSP is

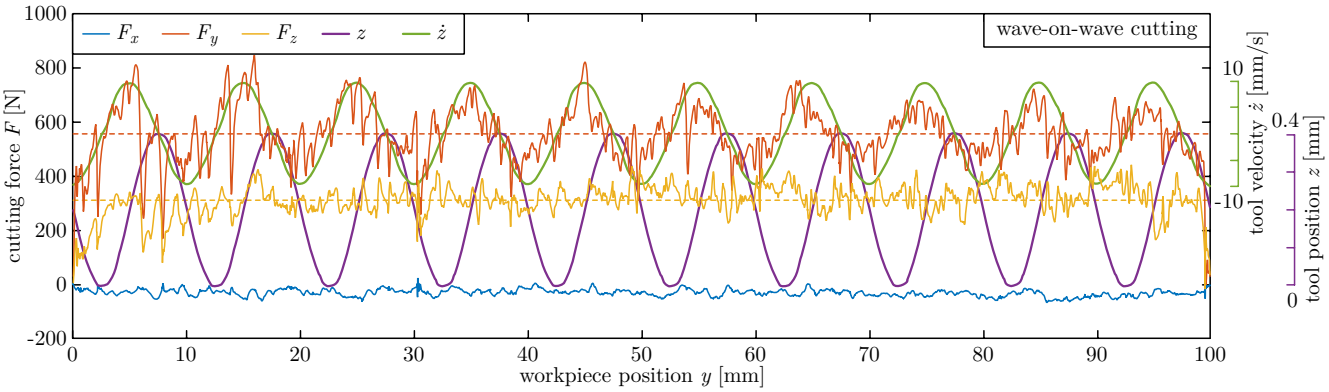

Figure 14: Cutting force signals of a wave-on-wave cutting experiment (see Fig. 2(d)). The corresponding tool position z and tool velocity $\dot{z}$ are also shown by purple and green lines for comparison. The cutting conditions are $\alpha_r = 2.5°$, $v_c = 5$ m/min, $h = 200\,\mu$m, $z_{amp} = 200\,\mu$m and $\lambda = 10$ mm.

unable to explain the phase shift since the velocity dependency is dropped in that case.

For wave removal, the geometrical explanation uses the phase shift between the shear plane length l and the uncut chip thickness h, which was demonstrated in Fig. 3. According to this explanation, there is no phase shift between the cutting force components and the shear plane length. Thus, if closed curves do not appear when plotting the cutting force characteristics against the shear plane length (i.e., if straight lines can be seen only), then it justifies the validity of this explanation. This plot can be found in Fig. 13(a,b) for the MSSP and the MEP shear angle models, respectively. Here, the shear plane length was obtained numerically from the realized tool path via the shear angle, which was calculated from Eqs. (12) and (13) using the average cutting force components.

Figure 13(a) shows the case of the MSSP. Here, the closed curves seemingly disappear from the measured cutting force characteristics (thin lines), but narrow closed curves are still visible in the averaged ones (thick lines). These closed curves run in the counter-clockwise direction, i.e., the opposite direction that was shown previously in Fig. 12. This indicates that the calculated shear plane length leads the measured cutting force components. That is, the MSSP overcompensates the phase shift: it predicts too small shear angle, which results in a larger phase shift between the shear plane length and the chip thickness than the one between the cutting force and the chip thickness. Note that a counter-clockwise closed curve in the characteristics would correspond to a negative additional damping in process damping models, which is a qualitatively different behavior from the one that is expected.

Meanwhile, the case of the MEP is shown in Fig. 13(b). Here, the closed curves are still present in the average characteristics (thick lines), but they are much narrower than in terms of the chip thickness in Fig. 12(b). In comparison to the case of the MSSP in Fig. 13(a), the closed curves are slightly wider, but they run in the clockwise direction, which is more meaningful for process damping models. Therefore, it can be concluded that the MEP shear angle model is in better agreement with the experiments than the MSSP both for wave generation and wave removal. Recall that the high-speed camera measurements during stationary cutting lead to the same conclusion in Sec. 4.

Furthermore, when applying the MEP, the cutting force versus shear plane length characteristics become qualitatively the same as the cutting force characteristics in stationary cutting. The results of the stationary cutting experiments (discussed and shown previously in Sec. 4, Fig. 6) are also indicated by dots in Fig. 12(a,b) and Fig. 13(a,b). The agreement between the stationary and non-stationary experiments is, again, slightly better when the MEP is chosen over the MSSP. Based on the good agreement of stationary and non-stationary results in Fig. 13(b), the cutting force characteristics can be determined from a single non-stationary experiment instead of a set of stationary ones.

6. Experimental Results for Double Sinusoidal Tool Paths

Finally, the results for synchronous wave-on-wave cutting experiments (corresponding to panel (d) of Fig. 2) are presented. Here, the same sinusoidal tool motion was performed twice and the second one was analyzed. That is, the waviness on the upper and lower chip surfaces were (nominally) the same and the nominal uncut chip thickness was constant in time ($\dot{h} = 0$). As the tool was moving up and down during cutting, the effect of fluctuations in the cutting direction could clearly be observed without involving variations of the nominal uncut chip thickness [19, 13].

A sequence of wave-on-wave cutting experiments were conducted with sinusoidal tool paths of wavelength $\lambda = 10$ mm and amplitudes $z_{amp} = 100,\ 150,\ 200\,\mu$m, which correspond to $\Delta\alpha_{amp} = 3.6°,\ 5.4°,\ 7.2°$ fluctuations in the cutting direction. The cutting speed was $v_c = 5$ m/min and the nominal uncut chip thickness values $h = 100\,\mu$m and $200\,\mu$m were prescribed.

Figure 14 presents the cutting force signal of a wave-on-wave cutting experiment, where the nominal rake angle of the tool was $\alpha_r = 2.5°$, while the amplitude of the tool path was $z_{amp} = 200\,\mu$m. Although the nominal uncut chip thickness was constant ($h = 200\,\mu$m), the cutting force components (especially F_y) show strong variations. For reference, a scaled value of the tool position z and a shifted and a scaled value

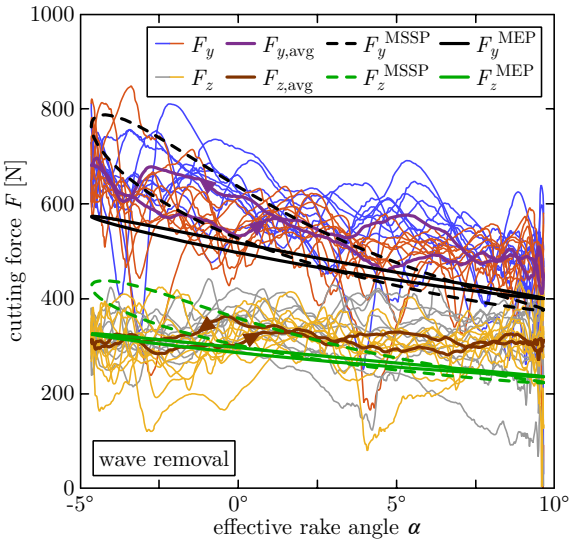

Figure 15: Cutting force components as a function of the fluctuating effective rake angle for a wave-on-wave cutting experiment. The cutting conditions are the same as in Fig. 14.

of the vibration velocity $\dot{z}$ are also shown in the figure. The cutting force component F_y is in approximately 90° phase shift with respect to the tool position and is almost in phase with the vibration velocity. The correlation of the cutting force with the vibration velocity shows that fluctuations in the cutting direction strongly affect the cutting force during dynamic chip formation.

It is shown below that primarily the effective rake angle fluctuations are responsible for the cutting force variations as predicted by the geometrical explanation in Sec. 2. Recall that in stationary cutting, the cutting force components typically decrease with increasing nominal rake angle (see Fig. 7(a) and Sec. 4). A similar tendency is expected for time-varying (fluctuating) effective rake angles. Thin lines in Fig. 15 show the components F_y and F_z of the cutting force versus the effective rake angle α for a wave-on-wave cutting experiment. Different colors distinguish cutting force components corresponding to increasing and decreasing effective rake angle. The nominal rake angle was $\alpha_r = 2.5°$, the amplitude of the tool path was $z_{\mathrm{amp}} = 200\,\mu$m, thus the effective rake angle was fluctuating with amplitude 7.2° between −4.7° and 9.7°. Apparently, the cutting force components decrease with increasing rake angle, similarly to stationary cutting. Experiments with different nominal rake angles have shown that the cutting force fluctuations are typically larger when the effective rake angle fluctuates around a smaller nominal value.

The decreasing tendency in Fig. 15 can be captured by the model of Sec. 2. Again, a key point is the geometrical explanation that the rake and shear angles fluctuate for a vibrating tool. In order to compare the theory to experiments, the cutting force components were calculated from Eq. (11) as a function of the effective rake angle for $-4.7° \le \alpha \le 9.7°$. To this end, the shear angle Φ was obtained from the MSSP and the MEP shear angle models (12) and (13), respectively. Based on the shear angle Φ, the shear plane length l was calculated from the prescribed tool paths. Besides, since the value of the shear stress τ_s in Eq. (11) was unknown, the average shear stress obtained from the stationary cutting experiments with $50\,\mu\mathrm{m} < h < 300\,\mu\mathrm{m}$ was used (that is, the effects of tool edge radius and strong segmentation were disregarded). The average shear stress values were $\tau_s = 262$ MPa for the MSSP and $\tau_s = 313$ MPa for the MEP. Similarly, the ploughing force was obtained from stationary cutting data, resulting in $P_y = 61.2$ N and $P_z = 57.7$ N. Finally, two different cutting forces were calculated: one for the MSSP and one for the MEP, whose components are depicted in Fig. 15 by thick dashed and thick solid lines, respectively.

Note that the shear plane length l is different for increasing and decreasing effective rake angles α (and their relationship is nonlinear). Thus, the theory predicts ellipse-shaped closed curves in Fig. 15 when plotting the cutting force components (that depend on the shear plane length) as a function of the fluctuating rake angle. Comparison of theory (thick lines) and experiment (thin lines) shows that the MEP shear angle model is able to accurately explain the tendency of cutting force fluctuations due to the variations of the effective rake angle. However, the cutting force is slightly underestimated by the model, possibly due to the discrepancy between the actual value of the shear stress τ_s and its value calculated from stationary cutting data. Meanwhile, the MSSP does not capture the tendency of the cutting force accurately: it gives a too wide closed curve with too large negative slope. Thus, even in the case of wave-on-wave cutting, the geometrical explanation provides a more accurate description of dynamic chip formation when it is supplemented by the MEP shear angle model rather than by the MSSP.

7. Conclusions

A set of orthogonal planing experiments was performed in order to investigate chip formation during machine tool vibrations. The cutting force was measured and the chip formation process was recorded via high-speed camera for stationary cutting and non-stationary (wave generation, wave removal and wave-on-wave cutting) experiments. The measured cutting force signals were compared to theoretical predictions. The theory uses a geometrical explanation: the cutting direction fluctuates for a vibrating tool, which affects the effective rake angle, the shear angle, the shear plane length and the effective chip thickness, while the surface waviness also causes variations in the shear plane length.

The main contributions of the paper are: (i) the application of the geometrical explanation to address cutting force fluctuations under dynamic cutting conditions; (ii) the assessment of shear angle models; (iii) the experimental observation of some key features of chip segmentation; (iv) the high-speed camera recording of the chip formation process. The experiments lead to the following conclusions for the investigated range of cutting parameters.

- In stationary cutting, the cutting force components typically increase with increasing uncut chip thickness. There is a break down in the feed force characteristics for large chip

thickness values due to the appearance of strong chip segmentation.

- The cutting force components typically decrease with increasing rake angle.
- The cutting speed has moderate effect on the cutting force (in the parameter ranges investigated).
- Chip segmentation is more likely to occur and is stronger for large uncut chip thickness, small cutting speed and small rake angle values. Its frequency increases with the cutting speed, but the corresponding wavelength is approximately constant.
- The occurrence of chip segmentation typically exhibits hysteresis with respect to the variation of the nominal uncut chip thickness in non-stationary cutting.
- The MSSP predicts smaller shear angle than the MEP does. In stationary cutting, the prediction of the MEP is the one that is closer to high-speed camera observations.
- In non-stationary cutting, there is a phase shift between the nominal uncut chip thickness and cutting force signals. The role of this phase shift is critical for understanding additional damping forces arising during machine tool vibrations (such as the process damping). The phase shift is typically larger for wave removal than for wave generation.
- The phase shift can well be explained geometrically by the fluctuation of the cutting direction in wave generation and by the lag between the shear plane length and the nominal uncut chip thickness in wave removal.
- The MEP shear angle model performs better than the MSSP does in predicting the phase shift.
- In non-stationary cutting, effective rake angle fluctuations cause variations in the cutting force. The variations are larger for small nominal rake angles, and the cutting force tends to decrease with increasing effective rake angle (similarly to stationary cutting).

The most important conclusion of this paper is that cutting force fluctuations can be accurately predicted by the geometrical explanation using the MEP shear angle model. According to this explanation, the cutting force during dynamic chip formation is determined rather by the effective cutting velocity than the nominal one, while the shear plane length is in stronger correlation with the cutting force than the nominal uncut chip thickness. The cutting force fluctuations investigated above can well be explained based on these principles, although the construction of an accurate shear angle model is critical. Here, the MEP was found to be a good candidate for appropriate shear angle model.

Note that these cutting force fluctuations may have significant role when analyzing the stability of cutting processes and the onset of machine tool chatter. In [60], the effective cutting direction was considered instead of the nominal one to analyze the stability of milling and to address the process damping phenomenon. Thus, the experimental results of the present paper justify that the initial assumptions of [60] were valid. However, it was shown in [60] that the fluctuations of the cutting direction alone cannot explain the improvement of stability at low cutting speeds for certain machining processes (such as low radial immersion milling). In these processes, other phenomena such as the flank contact [47, 56, 49, 57, 50, 53] or the distribution of the cutting force along the rake face [58, 59, 55] can be responsible for the low speed stability improvement. In this sense, the experimental results of this paper may help understanding the cause of the low speed stability improvement phenomenon, which facilitates the design of chatter-free cutting processes.

The experimental results can further be used to validate more sophisticated analytical models of chip formation [43] or the finite element analysis of orthogonal cutting processes. Our future research involves building high-fidelity finite element models of metal cutting, which are validated by the low speed experiments of this paper. The advantage of low speed cutting tests is that various wavy tool paths can be realized accurately in a well-controlled clean experimental environment. Such well-controlled tool motion is hard to achieve at high speeds. However, the high-fidelity finite element models enable the investigation of orthogonal cutting at high cutting speeds and with more severe oscillations of the tool, which is a more realistic representation of chatter in industrial practice. This method enables justifying the results of this paper at high speeds, which is an important step of future research work.

Acknowledgments

The research leading to these results has received funding from the European Research Council under the European Union's Seventh Framework Programme (FP/2007-2013) / ERC Advanced Grant Agreement n. 340889. This work has been supported by the ÚNKP-18-3-I. New National Excellence Program of the Ministry of Human Capacities. The research leading to these results was supported by the Hungarian Scientific Research Fund (OTKA FK-124462 and PD-124646). The research reported in this paper has been supported by the National Research, Development and Innovation Fund (TUDFO/51757/2019-ITM, Thematic Excellence Program).

References

[1] M. Wiercigroch, E. Budak, Sources of nonlinearities, chatter generation and suppression in metal cutting, Philosophical Transactions of the Royal Society A: Mathematical, Physical and Engineering Sciences 359 (1781) (2001) 663–693.

[2] P. Wahi, A. Chatterjee, Self-interrupted regenerative metal cutting in turning, International Journal of Non-Linear Mechanics 43 (2) (2008) 111–123.

[3] M. Azvar, E. Budak, Multi-dimensional chatter stability for enhanced productivity in different parallel turning strategies, International Journal of Machine Tools and Manufacture 123 (2017) 116–128.

[4] N. D. Sims, B. Mann, S. Huyanana, Analytical prediction of chatter stability for variable pitch and variable helix milling tools, Journal of Sound and Vibration 317 (3–5) (2008) 664–686.

[5] E. A. Butcher, O. Bobrenkov, E. Bueler, P. Nindujarla, Analysis of milling stability by the Chebyshev Collocation Method: algorithm and optimal stable immersion levels, Journal of Computational and Nonlinear Dynamics 4 (3) (2009) 031003 (12 pages).

[6] E. Ozturk, E. Budak, Dynamics and stability of five-axis ball-end milling, Journal of Manufacturing Science and Engineering 132 (2) (2010) 021003 (13 pages).

[7] G. Totis, P. Albertelli, M. Torta, M. Sortino, M. Monno, Upgraded stability analysis of milling operations by means of advanced modeling of tooling system bending, International Journal of Machine Tools and Manufacture 113 (2017) 19–34.

[8] X. Liu, N. Vlajic, X. Long, G. Meng, B. Balachandran, State-dependent delay influenced drill-string oscillations and stability analysis, Journal of Vibration and Acoustics 136 (5) (2014) 051008 (9 pages).

[9] Y. Yan, J. Xu, M. Wiercigroch, Regenerative chatter in a plunge grinding process with workpiece imbalance, International Journal of Advanced Manufacturing Technology 89 (9–12) (2016) 2845–2862.

[10] U. Yigit, E. Cigeroglu, E. Budak, Chatter reduction in boring process by using piezoelectric shunt damping with experimental verification, Mechanical Systems and Signal Processing 94 (2017) 312–321.

[11] A. Comak, Y. Altintas, Mechanics of turn-milling operations, International Journal of Machine Tools and Manufacture 121 (2017) 2–9.

[12] P. Albrecht, Dynamics of the metal-cutting process, Journal of Engineering for Industry 87 (4) (1965) 429–441.

[13] M. K. Das, S. A. Tobias, The relation between the static and the dynamic cutting of metals, International Journal of Machine Tool Design and Research 7 (2) (1967) 63–89.

[14] Y. Altintas, Manufacturing Automation - Metal Cutting Mechanics, Machine Tool Vibrations and CNC Design, Second Edition, Cambridge University Press, Cambridge, 2012.

[15] J. Hwang, S. Chandrasekar, Contact conditions at the chip-tool interface in machining, International Journal of Precision Engineering and Manufacturing 12 (2) (2011) 183–193.

[16] G. Sutter, A. Molinari, G. List, X. Bi, Chip flow and scaling laws in high speed metal cutting, ASME Journal of Manufacturing Science and Engineering 134 (2) (2012) 021005 (9 pages).

[17] Y. Guo, W. D. Compton, S. Chandrasekar, In situ analysis of flow dynamics and deformation fields in cutting and sliding of metals, Proceedings of the Royal Society A - Mathematical, Physical and Engineering Sciences 471 (2178) (2015) 20150194 (18 pages).

[18] S. Berezvai, D. Bachrathy, G. Stepan, High-speed camera measurements in the mechanical analysis of machining, in: Proceedings of the 8th CIRP Conference on High Performance Cutting, Vol. 77, Budapest, Hungary, 2018, pp. 155–158.

[19] P. W. Wallace, C. Andrew, Machining forces: Some effects of tool vibration, Journal of Mechanical Engineering Science 7 (2) (1965) 152–162.

[20] M. Masuko, J. Kumabe, T. Tsukada, Experimental study on the instantaneous cutting forces in metal cutting with oscillating tools, Bulletin of Japan Society of Mechanical Engineers 9 (33) (1966) 209–216.

[21] M. M. Nigm, M. M. Sadek, Experimental investigation of the characteristics of dynamic cutting process, Journal of Engineering for Industry 99 (2) (1977) 410–418.

[22] M. M. Nigm, M. M. Sadek, S. A. Tobias, Dimensional analysis of the steady state orthogonal cutting process, International Journal of Machine Tool Design and Research 17 (1) (1977) 1–18.

[23] M. M. Nigm, M. M. Sadek, S. A. Tobias, Determination of dynamic cutting coefficients from steady state cutting data, International Journal of Machine Tool Design and Research 17 (1) (1977) 19–37.

[24] J. L. Cantero, J. Díaz-Álvarez, D. Infante-García, M. Rodríguez, V. Criado, High speed finish turning of Inconel 718 using PCBN tools under dry conditions, Metals 8 (3) (2018) 192.

[25] Y. S. Ahmed, J. M. Paiva, B. Bose, S. C. Veldhuis, New observations on built-up edge structures for improving machining performance during the cutting of superduplex stainless steel, Tribology International 137 (2019) 212–227.

[26] T. Insperger, G. Stepan, J. Turi, State-dependent delay in regenerative turning processes, Nonlinear Dynamics 47 (1–3) (2007) 275–283.

[27] M. M. Nigm, M. M. Sadek, S. A. Tobias, Prediction of dynamic cutting coefficients from steady-state cutting data, in: Proceedings of the 13th International Machine Tool Design and Research Conference, London, UK, 1973, pp. 3–12.

[28] D. W. Wu, Comprehensive dynamic cutting force model and its application to wave-removing processes, Journal of Engineering for Industry 110 (2) (1988) 153–161.

[29] D. W. Wu, A new approach of formulating the transfer function for dynamic cutting processes, Journal of Engineering for Industry 111 (1) (1989) 37–47.

[30] P. Albrecht, New developments in the theory of the metal-cutting process: Part I. The ploughing process in metal cutting, Journal of Engineering for Industry 82 (4) (1960) 348–357.

[31] D. W. Wu, C. R. Liu, An analytical model of cutting dynamics. Part 1: Model building, Journal of Engineering for Industry 107 (2) (1985) 107–111.

[32] D. W. Wu, Prediction of shear angle variation in orthogonal wave-removing processes, International Journal of Machine Tools and Manufacture 27 (3) (1986) 289–304.

[33] M. Hayajneh, V. Astakhov, M. Osman, An analytical evaluation of the cutting forces in orthogonal cutting using a dynamic model of the shear zone with parallel boundaries, Journal of Materials Processing Technology 82 (1–3) (1998) 61–77.

[34] D. W. Wu, Governing equations of the shear angle oscillation in dynamic orthogonal cutting, Journal of Engineering for Industry 108 (4) (1986) 280–287.

[35] R. L. Kegg, Cutting dynamics in machine tool chatter: Contribution to machine-tool chatter research–3, Journal of Engineering for Industry 87 (4) (1965) 464–470.

[36] S. Berezvai, T. G. Molnar, D. Bachrathy, G. Stepan, Experimental investigation of the shear angle variation during orthogonal cutting, Materials Today: Proceedings 5 (13) (2018) 26495–26500.

[37] S. Berezvai, T. G. Molnar, A. Kossa, D. Bachrathy, G. Stepan, Numerical and experimental investigation of contact length during orthogonal cutting, Materials Today: Proceedings 12 (2) (2019) 329–334.

[38] D. Bachrathy, G. Stepan, Cutting force measurements in high speed milling: Extension of the frequency range of Kistler dynamometer, in: Proceedings of the 39th International MATADOR Conference on Advanced Manufacturing, no. 0033, Manchester, UK, 2017.

[39] E. M. Trent, P. K. Wright, Metal Cutting, Butterworth-Heinemann, Boston, 2000.

[40] Z. Palmai, Chaotic phenomena induced by the fast plastic deformation of metals during cutting, Journal of Applied Mechanics 73 (2) (2006) 240–245.

[41] Z. Palmai, G. Csernak, Chip formation as an oscillator during the turning process, Journal of Sound and Vibration 326 (3-5) (2009) 809–820.

[42] G. Csernak, Z. Palmai, Exploration of the chaotic phenomena induced by fast plastic deformation of metals, International Journal of Advanced Manufacturing Technology 40 (3–4) (2009) 270–276.

[43] G. Gyebroszki, D. Bachrathy, G. Csernak, G. Stepan, Stability of turning processes for periodic chip formation, Advances in Manufacturing 6 (3) (2018) 345–353.

[44] W. J. Endres, M. Loo, Modeling cutting process nonlinearity for stability analysis - application to tooling selection for valve-seat machining, in: Proceedings of the 5th CIRP International Workshop on Modeling of Machining, West Lafayette, IN, USA, 2002, pp. 71–82.

[45] G. Stepan, D. Hajdu, A. Iglesias, D. Takacs, Z. Dombovari, Ultimate capability of variable pitch milling cutters, CIRP Annals - Manufacturing Technology 67 (1) (2018) 373–376.

[46] V. P. Astakhov, On the inadequacy of the single-shear plane model of chip formation, International Journal of Mechanical Sciences 47 (11) (2005) 1649–1672.

[47] B. E. Clancy, Y. C. Shin, A comprehensive chatter prediction model for face turning operation including tool wear effect, International Journal of Machine Tools and Manufacture 42 (9) (2002) 1035–1044.

[48] D. Bachrathy, G. Stepan, Time-periodic velocity-dependent process damping in milling processes, in: Y. Altintas, B. Denkena, C. Brecher (Eds.), Proceedings of the 2nd International CIRP Conference on Process Machine Interaction, Vancouver, Canada, 2010, pp. 1–12.

[49] E. Budak, L. T. Tunc, Identification and modeling of process damping in turning and milling using a new approach, CIRP Annals - Manufacturing Technology 59 (1) (2010) 403–408.

[50] K. Ahmadi, F. Ismail, Stability lobes in milling including process damping and utilizing multi-frequency and semi-discretization methods, International Journal of Machine Tools and Manufacture 54–55 (2012) 46–54.

[51] V. Sellmeier, B. Denkena, High speed process damping in milling, CIRP Journal of Manufacturing Science and Technology 5 (1) (2012) 8–19.

[52] C. T. Tyler, T. L. Schmitz, Analytical process damping stability prediction, Journal of Manufacturing Processes 15 (1) (2013) 69–76.

[53] X. Jin, Identification of process damping coefficient based on material constitutive property, in: Proceedings of the ASME International Manufacturing Science and Engineering Conference, no. MSEC2014–4204, Detroit, MI, USA, 2014, pp. 1–7.
[54] Z. Dombovari, D. A. Barton, R. E. Wilson, G. Stepan, On the global dynamics of chatter in the orthogonal cutting model, International Journal of Non-Linear Mechanics 46 (1) (2011) 330–338.
[55] Z. Dombovari, G. Stepan, Experimental and theoretical study of distributed delay in machining, in: Proceedings of the 9th IFAC Workshop on Time Delay Systems, Prague, Czech Republic, 2010, pp. 1–5.
[56] Y. Altintas, M. Eynian, H. Onozuka, Identification of dynamic cutting force coefficients and chatter stability with process damping, CIRP Annals - Manufacturing Technology 57 (1) (2008) 371–374.
[57] M. Eynian, Y. Altintas, Analytical chatter stability of milling with rotating cutter dynamics at process damping speeds, ASME Journal of Manufacturing Science and Engineering 132 (2) (2010) 021012 (14 pages).
[58] G. Stepan, Delay-differential equation models for machine tool chatter, in: F. C. Moon (Ed.), Dynamics and Chaos in Manufacturing Processes, John Wiley and Sons, New York, 1997, pp. 165–192.
[59] F. A. Khasawneh, B. P. Mann, T. Insperger, G. Stepan, Increased stability of low-speed turning through a distributed force and continuous delay model, Journal of Computational and Nonlinear Dynamics 4 (4) (2009) 041003 (12 pages).
[60] T. G. Molnar, T. Insperger, D. Bachrathy, G. Stepan, Extension of process damping to milling with low radial immersion, International Journal of Advanced Manufacturing Technology 89 (9) (2017) 2545–2556.